

## MORPHOLOGICAL &amp; DYNAMICAL PROPERTIES OF LOW REDSHIFT 2DFGRS GROUPS

M. PLIONIS<sup>1,2</sup>, S. BASILAKOS<sup>1,3</sup>, C. RAGONE-FIGUEROA<sup>4,5</sup>*Draft version April 22, 2018*

## ABSTRACT

We estimate the average group morphological and dynamical characteristics of the Percolation-Inferred Galaxy Group (2PIGG) catalogue within  $z \leq 0.08$ , for which the group space density is roughly constant. We quantify the different biases that enter in the determination of these characteristics and we devise statistical correction procedures to recover their bias free values. We find that the only acceptable morphological model is that of prolate, or triaxial with pronounced prolateness, group shapes having a roughly Gaussian intrinsic axial ratio distribution with mean  $\sim 0.46$  and dispersion of  $\sim 0.16$ . After correcting for various biases, the most important of which is a redshift dependant bias, the median values of the virial mass and virial radius of groups with 4 to 30 galaxy members, is:  $\overline{M}_v \sim 6 \times 10^{12} h_{72}^{-1} M_\odot$ ,  $\overline{R}_v \sim 0.4 h_{72}^{-1}$  Mpc, which are significantly smaller than recent literature values that do not take into account the previously mentioned biases. The group mean crossing time is  $\sim 1.5$  Gyr's, independent of the group galaxy membership. We also find that there is a correlation of the group size, velocity dispersion and virial mass with the number of group member galaxies, a manifestation of the hierarchy of cosmic structures.

*Subject headings:* galaxies: clusters: general

## 1. INTRODUCTION

Groups of galaxies are the lowest level cosmic structures, after galaxies themselves, in the hierarchy that leads to the largest virialized structures, the clusters of galaxies. There have been a number of recent attempts to construct objectively selected group and cluster catalogues from magnitude limited redshift or photometric galaxy surveys, like the combination of the Updated Zwicky Catalogue and the Southern Sky Redshift Survey (UZC-SSRS2), the Sloan digital sky survey (SDSS), the two-degree field redshift survey (2dFRGS), the digital Palomar observatory sky survey; eg., Ramella et al (2002); Merchán & Zandivarez (2002, 2005); Gal et al. (2003); Bachall et al. (2003); Goto et al. (2004); Lee et al. (2004); Lopes et al. (2004); Eke et al. (2004); Tago et al (2006); Berlind et al (2006). Most of the studies that use galaxy redshift information, apply the so-called friends-of-friends algorithm (FoF) to the galaxy redshift data by using a variable linking length that takes into account the drop of the redshift selection function with increasing redshift.

It appears that most galaxies are found in groups and they are therefore extremely important in our attempts to understand the cosmic structure formation processes. Since virialization will tend to sphericalize initial anisotropic distributions of matter, the shape of different cosmic structures is an indication of their evolutionary stage. Furthermore, the group shape, size and velocity dispersion are important factors in determining galaxy member orbits and interaction rates, which are instrumental in understanding galaxy evolution processes. A lot of theoretical and observational studies have dealt with the intrinsic shape of cosmic structures and their dependence on

different cosmological backgrounds, environments, evolutionary stage, etc. (e.g., Carter & Metcalfe 1980; Plionis, Barrow & Frenk 1991; Cooray 2000; Basilakos, Plionis & Maddox 2000; Zeldovich, Einasto & Shandarin 1982; de Lapparent, Geller & Huchra 1991; Plionis, Valdarnini & Jing 1992; Oleak et al. 1995; de Theije, Katgert & van Kampen 1995; Jaaniste et al. 1998; Sathyaprakash et al. 1998; Valdarnini, Ghizzardi & Bonometto 1999; Basilakos, Plionis & Rowan-Robinson 2001; Jing & Suto 2002; Kasun & Evrard 2005; Allgood et al. 2006; Paz et al. 2006; Sereno et al. 2006). In the case of groups of galaxies a study of the UZC-SSRS2 group catalogue (Plionis, Basilakos & Tovmassian 2004) have shown that they are quite elongated prolate-like systems.

In this paper we use the recently constructed 2PIGG group catalogue (Eke et al. 2004), based on the 2-degree field redshift survey, to estimate the group projected and intrinsic shape, size, velocity dispersion, virial mass and crossing-time distributions after correcting for a number of systematic biases.

## 2. GROUP SAMPLE SELECTION

The 2PIGG group catalogue (Eke et al. 2004) is constructed by applying a friends-of-friends (FoF) algorithm to the two degree field galaxy redshift survey (2dFRGS), which contains 191440 galaxies with well defined magnitude and redshift selection functions. The FoF linking parameters were selected after thorough tests that have been applied on mock  $\Lambda$ CDM galaxy catalogues. The resulting 2PIGG group catalogue contains 7020 groups with at least 4 members having a median redshift of 0.11.

The specific group finding algorithm used (Eke et al. 2004) treats in detail many issues that are related to com-

<sup>1</sup> Institute of Astronomy & Astrophysics, National Observatory of Athens, Palaia Penteli 152 36, Athens, Greece

<sup>2</sup> Instituto Nacional de Astrofísica Óptica y Electrónica, AP 51 y 216, 72000, Puebla, Pue, México

<sup>3</sup> Research Center for Astronomy & Applied Mathematics, Academy of Athens, Soranou Efessiou 4, GR-11527 Athens, Greece

<sup>4</sup> Grupo IATE-Observatorio Astronómico, Laprida 854, Córdoba, Argentina

<sup>5</sup> Consejo de Investigaciones Científicas y Técnicas de la Rep'ublica Argentina, Córdoba, Argentina

pleteness, the underlying galaxy selection function and the resulting biases that enter in attempts to construct unbiased group or cluster catalogues.

In order to take into account the drop of the underlying galaxy number density with redshift, due to its magnitude limited nature, Eke et al. (2004) have used a FoF linking parameter that scales with redshift. The redshift scaling of this parameter is variable in the perpendicular and also parallel to the line-of-sight direction, with their ratio being  $\sim 11$ . The necessity to increase the linking volume with redshift introduces, however, biases in the morphological and dynamical characteristics of the resulting groups which should be taken into account before attempting to derive their physical and morphological properties. For example, an outcome of the above group finding algorithm is the increase with redshift of both the velocity dispersion and the projected size of the candidate groups. Such a systematic effect was also found in the Ramella et al (2002) group catalogue by Plionis et al (2004).

In Fig.1 we present the group velocity dispersion and a measure of their projected size as a function of group redshift (for groups with membership  $n_m \geq 4$ ). The group projected size, related to the virial radius, is found by:

$$r = \frac{n_m(n_m - 1)}{2} \left[ \sum_{i=1}^{n_m-1} \sum_{j=i+1}^{n_m} \frac{1}{D_L \tan(c_{ij} \delta\theta_{ij})} \right]^{-1}, \quad (1)$$

where  $D_L$  is the luminosity distance of the group within the concordance Cosmological model ( $\Omega_\Lambda = 0.7$ ,  $\Omega_m = 0.3$ ,  $h_{72} = 0.72$ ),  $\delta\theta_{ij}$  is the angular  $(i, j)$ -pair separation and  $c_{ij}$  is an average galaxy pair weight that takes into account the variable 2dFGRS incompleteness (in angular, redshift and magnitude limit space). The individual galaxy weights are taken from Eke et al. (2004). Note that the above measure of the size is significantly smaller than the maximum group galaxy-pair separation,  $r_{\max}$ .

A strong redshift dependence is evident in Fig.1. The larger velocity dispersion of high- $z$  groups could be possibly attributed to the fact that we tend to observe at large redshifts only the richest groups (due to the flux-limited nature of the 2dFGRS). However, the fact that the projected group size and velocity dispersion increases monotonically with redshift, while the large and high- $\sigma_v$  groups are not found at lower redshifts, can be attributed only to the group identification method (for a thorough discussion of  $z$ -dependent effects of the FoF algorithm see Frederic 1995 and Diaferio et al. 1999).

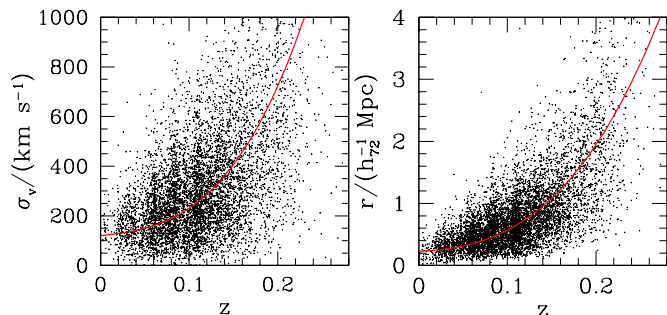


FIG. 1.— The dependence of the group velocity dispersion (left panel) and the group size (right panel) on redshift. The solid lines are  $3^{rd}$  order polynomial fits.

Therefore, the probability that the groups found are true dynamical entities decreases with increasing redshift, but even if the high- $z$  groups are real (but contaminated) entities, they would constitute a different family of cosmic structures than the lower- $z$  ones. One can attempt to take into account such systematic biases by applying the same group finding algorithm on N-body simulations, the results of which can then be used to calibrate the statistical results based on the real data (eg. Eke et al. 2004).

Since, however, in this study we are interested in deriving the physical characteristics of the observed groups, we will attempt to quantify and minimize the various systematic biases. To this end we also limit the 2PIGG sample to within a redshift of  $z \simeq 0.08$ , a limit within which the density of groups (estimated in equal volume shells) is roughly constant, as can be seen in Figure 2.

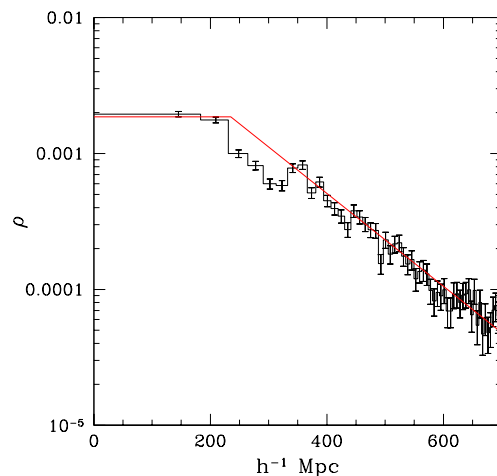


FIG. 2.— The group space density as a function of distance, estimated in equal volume shells. The straight line delineates the range where the density is roughly constant. The error-bars are  $2\sigma$  Poisson uncertainties.

We are finally left with 1948  $n_m \geq 4$  2PIGG groups, out of which 1788 have velocity dispersion estimates from Eke et al. (2004).

### 3. GROUP PROJECTED & INTRINSIC SHAPES

We derive the group projected axial ratio,  $q$ , by diagonalizing the two-dimensional inertia tensor (eg. Carter & Metcalfe 1983), which fits the best ellipse on the projected discrete distribution of galaxy group members. In Fig.3 (left panel) we present the group median axial ratio as a function of group membership (open circles). An interesting trend is apparent with  $\bar{q}$  increasing with increasing  $n_m$ , while it appears that for  $n_m \gtrsim 25$  the value of  $\bar{q}$  converges to a final value of  $\sim 0.56$ . We have verified that this correlation is not due to the increase with redshift of the group linking volume, which induces the systematic trend seen in Fig. 1.

#### 3.1. Sampling Effects

Discreteness effects have been found to affect the group shapes by artificially increasing ellipticities with decreasing sampling (Paz et al. 2006). We therefore ask the question, what would the mean axial-ratio be of groups, having intrinsic flattening that of the richest 2PIGG groups (ie.,  $\bar{q} \simeq 0.56$ ,  $n_m \geq 25$ ), when sampled with a smaller number

of points? To answer this question we use Monte-Carlo simulations to construct a large number ( $N_{sim} = 30000$  for each  $n_m$ ) of spheroidal 3D groups having a Gaussian distribution of intrinsic axial ratios,  $\beta$ , which we then sample with  $n_m$  random points. The mean and variance of the Gaussian is chosen, using a trial and error method, such that the corresponding median projected axial ratio, at the limit of dense sampling, is compatible with that of the richest 2PIGG groups. This is accomplished for a prolate or oblate spheroidal model, with  $\langle\beta\rangle \simeq 0.47$  and  $\langle\beta\rangle \simeq 0.20$ , respectively, while  $\sigma_\beta \simeq 0.20$  for both. Note, that since the Gaussian is bounded between  $0 \leq \beta \leq 1$ , different values of  $\sigma_\beta$  can indeed affect the resulting median projected group axial ratio.

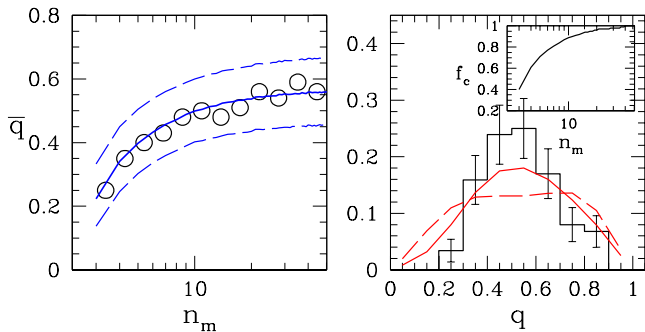


FIG. 3.— The correlation between the 2PIGG group “richness” ( $n_m$ ) and their median projected axial ratio (points). The solid line represent the expected distribution due to sampling effects (see text). Broken lines are the 33% and 67% quantiles of the corresponding distribution. The right panel shows the distribution of axial ratios of 2PIGG groups with  $19 \leq n_m \leq 25$  (histogram) and the corresponding Monte-Carlo prolate (continuous line) and oblate (dashed line) groups. The insert shows the correction factor with which we need to divide the raw group axial ratios in order to take into account the discreteness bias.

Then each group is randomly oriented with respect to the line of sight, the group members are projected on a surface and the projected axial ratio is measured. The outcome of the simulations give for  $n_m \gtrsim 20$  a median value of  $\bar{q} \simeq 0.54^{+0.05}_{-0.04}$  (showing that a sampling of 20 points per spheroid is adequate to recover the input axial ratio). The complete run as a function of  $n_m$  can be seen as the continuous line in Fig.3 (left panel), from which it is evident that the 2PIGG  $n_m - \bar{q}$  correlation (open symbols) is reproduced exactly (using either the prolate or oblate model for the Monte-Carlo groups). However, the distribution of the projected 2PIGG axial ratios was found to be in relatively good agreement only with that corresponding to the Monte-Carlo prolate groups. For example, in the right panel of Fig.3 we plot the axial ratio distribution of 2PIGG groups with  $19 \leq n_m \leq 25$  (histogram) and of the corresponding Monte-Carlo groups for the two spheroidal models (continuous and dashed lines).

This proves beyond any doubt that discreteness effects are the cause of the observed  $n_m - \bar{q}$  correlation and that the 2PIGG axial ratio distribution is more consistent with that of a prolate rather than an oblate three-dimensional model. Therefore, this analysis which serves to clarify the effects of sampling on the projected group shape, also hints on the intrinsic morphology of the 2PIGG groups, which formally will be derived in the next section.

In the insert of the right panel of Fig. 3 we plot the cor-

rection factor,  $f_c$ , derived from this analysis with which we need to divide the raw group axial ratios in order to neutralize the discreteness bias discussed before. Although we correct accordingly all the group raw axial ratios we will use the richest ( $n_m \geq 10$ ) 2PIGG groups, for which the discreteness correction is relatively small, to determine their intrinsic group shape distribution. We also put an upper limit to  $n_m$  ( $= 30$ ), in order to exclude from our morphological analysis clusters of galaxies, which may have a different dynamical history and thus a different shape distribution (for cluster shapes see Basilakos, Plionis & Maddox 2000 and references therein).

### 3.2. Recovering the Intrinsic Axial Ratio Distribution

An interesting question is whether the group 3D shape distribution can be inferred from the projected one. This is an inversion problem for which, under the assumption of random group orientation with respect to the line of sight and of purely oblate or prolate spheroidal shapes, there is a unique inversion. The problem is described by a set of integral equations, first investigated by Hubble (1926) and given by Sandage, Freeman & Stokes (1970) :

$$f(q) = \frac{1}{q^2} \int_0^q \frac{\beta^2 \hat{N}_p(\beta) d\beta}{(1-q^2)^{1/2} (q^2 - \beta^2)^{1/2}} \quad \text{prolate} \quad (2)$$

$$f(q) = q \int_0^q \frac{\hat{N}_o(\beta) d\beta}{(1-q^2)^{1/2} (q^2 - \beta^2)^{1/2}} \quad \text{oblate} \quad (3)$$

with  $\hat{N}_o(\beta)$  and  $\hat{N}_p(\beta)$  the intrinsic oblate and prolate axial ratio distributions, respectively, and  $f(q)$  the corresponding projected distribution. The continuous function  $f(q)$  is derived from the discrete axial ratios frequency distribution using the so-called kernel estimators (for details see Ryden 1996 and references therein). Although we will not review this method we note that the basic kernel estimate of the frequency distribution is defined as:

$$\hat{f}(q) = \frac{1}{Nh} \sum_i^N K\left(\frac{q - q_i}{h}\right), \quad (4)$$

where  $q_i$  are the group axial ratios and  $K(t)$  is the kernel function (assumed here to be a Gaussian), defined so that  $\int K(t) dt = 1$ , and  $h$  is the “kernel width” which determines the balance between smoothing and noise in the estimated distribution. The value of  $h$  is chosen so that the expected value of the integrated mean square error between the true,  $f(q)$ , and estimated,  $\hat{f}(q)$ , distributions is minimised (eg., Vio et al. 1994; Tremblay & Merritt 1995). Inverting then the above equations gives us the distribution of true axial ratios as a function of  $\hat{f}(q)$  (eg. Fall & Frenk 1983):

$$\hat{N}_o(\beta) = \frac{2\beta(1-\beta^2)^{1/2}}{\pi} \int_0^\beta \frac{d}{dq} \left( \frac{\hat{f}}{q} \right) \frac{dq}{(\beta^2 - q^2)^{1/2}} \quad (5)$$

and

$$\hat{N}_p(\beta) = \frac{2(1-\beta^2)^{1/2}}{\pi\beta} \int_0^\beta \frac{d}{dq} (q^2 \hat{f}) \frac{dq}{(\beta^2 - q^2)^{1/2}} \quad (6)$$

with  $\hat{f}(0) = 0$ . Integrating numerically eq.(5) and eq.(6) allowing  $\hat{N}_p(\beta)$  and  $\hat{N}_o(\beta)$  to take any value, we can derive the inverted (3D) axial ratio distributions. If groups are a mixture of the two spheroidal populations or they

are triaxial ellipsoids there is no unique inversion (Plionis, Barrow & Frenk 1991). However, all may not be lost and although the exact shape distribution may not be recovered accurately one could possibly infer whether the 3D halo shapes are predominantly more prolate or oblate-like.

### 3.3. Testing the method with $N$ -body simulations

Here we attempt to investigate the accuracy of the shape inversion method when the intrinsic 3D shape distribution is not that of pure spheroids. To this end we use GADGET2 (Springel et al. 2005) to run a large ( $L = 500 h^{-1}$  Mpc,  $N_p = 512^3$  particles)  $N$ -body (DM only) simulation of a flat low-density cold dark matter model with a matter density  $\Omega_m = 1 - \Omega_\Lambda = 0.3$ , Hubble constant  $H_0 = 72 \text{ km s}^{-1} \text{ Mpc}^{-1}$  and a normalization parameter of  $\sigma_8 = 0.9$ . The particle mass is  $m_p \geq 7.7 \times 10^{10} h^{-1} M_\odot$  comparable to the mass of one single galaxy. The halos are defined using a FoF algorithm with a linking length given by  $l = 0.17 \langle n \rangle^{-1/3}$  where  $\langle n \rangle$  is the mean density. This linking length corresponds to an overdensity  $\simeq 330$  at the present epoch ( $z = 0$ ). We will use intermediate richness halos with  $6 \times 10^{13} h^{-1} M_\odot \leq M_h \leq 8 \times 10^{13} h^{-1} M_\odot$ , for which there are more than 700 particles per halo and which therefore are free of discreteness effects. The total number of such halos is 2610.

Dark matter halo shapes are quantified using the so called triaxiality index (Franx, Illingworth, G., de Zeeuw 1991), defined as:  $T = (a^2 - b^2)/(a^2 - c^2)$  (with  $a, b, c$  are the major, intermediate and minor halo axes of the best fit ellipsoid) which has limiting values of  $T = 1$  (prolate spheroid) and  $T = 0$  (oblate spheroid). Our results, which are in agreement with other studies, show that the fraction of halos with pronounced prolateness (ie., large  $T$ s) is significantly higher than that of oblate-like halos. Overall we obtain from our simulated halos that  $\langle T \rangle \simeq 0.73$ .

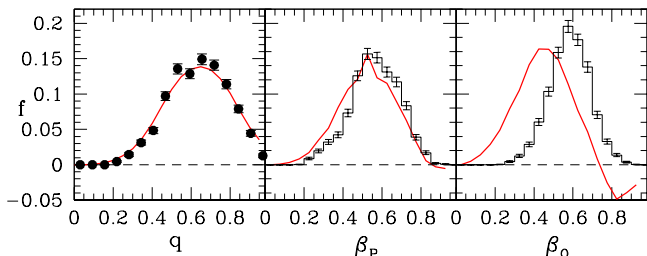


FIG. 4.— *Left panel:* The projected halo axial ratio distribution (points) and the smooth fit from the nonparametric kernel estimator (solid line). *Central & right Panels:* Comparison of the inverted intrinsic halo axial ratio distribution (continuous line) with the distribution of “average” spheroidal fits to the 3D halos (histograms), either for the prolate (central panel) or oblate (right panel) models.

We now project into 2D the distribution of halo particles and determine their projected axial ratios following the same procedure as in the real group data. In Fig.4 (left panel) we present the discrete and continuous -  $f(q)$  - distributions of the projected in 2D halo axial ratios. In the central and right panels we present the inverted 3D axial ratio distributions (continuous lines) for the prolate and oblate models, respectively. It is evident that the inverted oblate-model distribution is unacceptable due to the many negative values (at large  $\beta$ 's), while the opposite is true for the prolate-model distribution.

As a further test, we plot as histograms the intrinsic axial ratio distribution of the “average” prolate or oblate spheroidal fits to the 3D halos. These fits are realized by estimating the corresponding axial ratios by  $\beta_P = (b + c)/2a$  and  $\beta_O = 2c/(a + b)$ . It is evident that the purely oblate model fails miserably to even come close to the inverted distribution while the prolate model fits relatively well the corresponding inverted 3D prolate-model distribution. These results are in accordance with the intrinsic halo shapes determined in 3D, which were found to have a higher prolateness, as discussed previously.

We therefore conclude that applying the previously discussed inversion method to observational data we can infer, even in the event of triaxial ellipsoidal halo shapes, the dominance of prolate or oblate-like 3D shapes, if such does exist.

### 3.4. 2PIGG Intrinsic Shape

In Figure 5 (left panel) we present the raw and discreteness corrected projected axial ratio distributions for the 2PIGG groups with  $10 \leq n_m \leq 30$  (circles) with their Poisson  $1\sigma$  error bars, while the solid lines shows the continuous fits,  $f(q)$ . The median discreteness corrected axial ratio is  $\bar{q} = 0.55 \pm 0.08$ , while the uncorrected one is  $\sim 0.51$ .

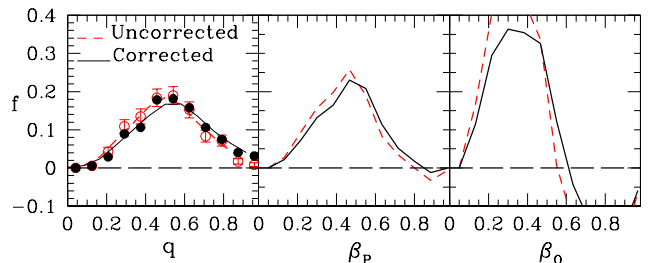


FIG. 5.— *Left panel:* The 2PIGG projected group axial ratio distribution (points) and the smooth fit from the nonparametric kernel estimator (lines), for the discreteness corrected case (filled points and continuous line) and the uncorrected case (open points and dashed line). *Central & right Panels:* The inverted intrinsic halo axial ratio distribution for the prolate (central panel) and oblate (right panel) cases.

In the central and left panels of Figure 5 we present the inverted intrinsic axial ratio distribution. The oblate model is completely unacceptable since it produces many negative values (at large  $\beta$ 's), while the prolate model fits quite-well, providing a roughly Gaussian intrinsic axial ratio distribution with  $\langle \beta \rangle \simeq 0.46$  and  $\sigma_\beta \simeq 0.16$  (which are also in very good agreement with the results of the Monte-Carlo procedure of section 3.1). Taking into account also the  $N$ -body simulation analysis of section 3.3, our results imply that the 2PIGG group shapes is well represented only by that of triaxial ellipsoids with a pronounced prolateness, which is also in agreement with the previous analysis of poor groups (Plionis et al. 2004), and compact groups (eg. Oleak et al. 1995).

## 4. GROUP DYNAMICAL CHARACTERISTICS

We are now interested in determining the typical size, velocity dispersion, crossing time and virial mass of the 2PIGG groups. We remind the reader of the strong  $z$ -dependence of these parameters (Fig.1) which is due to the group finding algorithm. Although, we have limited

our analysis to 2PIGG groups within  $z = 0.08$ , we observe that even within this  $z$ -limit, the previously discussed redshift dependant bias, although relatively weak, is still present (between  $z \simeq 0$  and  $z = 0.08$  the average values of  $\sigma_v$  and  $r$  increase by  $\sim 50\%$ ). In order to statistically correct for this bias we fitted third order polynomial functions,  $V(\sigma_v, z)$  and  $S(r, z)$ , to the data (solid curves in Fig.1) and then corrected the raw  $\sigma_v$  and  $r$  values by weighting them with  $V(\sigma_v, 0)/V(\sigma_v, z)$  and  $S(r, 0)/S(r, z)$ , respectively. However, we present results also for the very local volume ( $z \leq 0.03$ ) which apparently is unaffected by the redshift dependent bias (see Table 1).

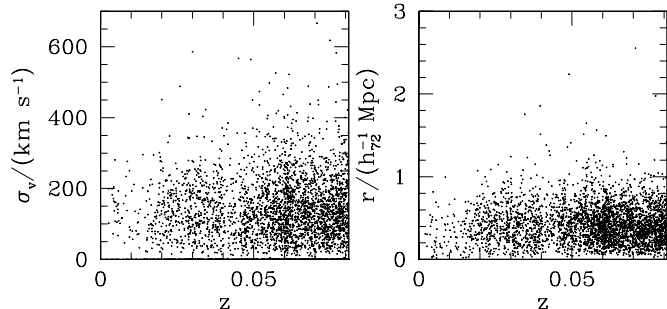


FIG. 6.— The dependence of the corrected group velocity dispersion (left panel) and group size (right panel) on redshift.

Also, due to the discreteness effects, quantified in section 3.1, there is an enhancement of the projected group size,  $r$ , especially at small  $n_m$ 's (eg. we find a  $\sim 18\%$  increase of the projected size for groups with  $n_m = 4$ ). For the velocity dispersion case we sample a Gaussian velocity distribution with  $n_m$  and we find a generally small effect (eg. there is a  $\sim 10\%$  reduction of  $\sigma_v$  for groups with  $n_m = 4$ ). In Fig.6 we present the corrected, for all the above biases, group velocity dispersion and size as a function of redshift for our  $z \leq 0.08$  sample. It is evident that the strong dependence on redshift has been eradicated and although the individual values of velocity dispersion and size may diverge from the intrinsic values, the overall population statistics should be correct.

After applying the above corrections to the group velocity dispersion and size, we can estimate their virial mass and crossing time by:

$$M_v = \frac{3\sigma_v^2 R_v}{G}, \quad \tau = \frac{R_v}{\sqrt{3}\sigma_v}, \quad (7)$$

where the group virial radius is  $R_v = (\pi/2)r$  (with  $r$  given by eq.1). In Table 1 we present the median values of these parameters, as well as the maximum projected group intergalaxy separation ( $r_{\max}$ ), for the bias corrected sample (with  $z \leq 0.08$ ), for the unaffected by the bias very local sample ( $z \leq 0.03$ ), as well as for two different redshift-limited samples, but with no corrections applied in order to appreciate the extend of the biases (note that the dominant correction is by far that of the redshift dependence). The comparison of these results yields that:

- (a) the effect of correcting the  $z \leq 0.08$  groups is appreciable, while the corrected median values of  $M_v$  and  $R_v$  are about equal to those of the local ( $z \leq 0.03$ ), unaffected by biases, sample, and
- (b) the effect is extremely large when using groups of any redshift (the uncorrected median values of  $M_v$  and  $R_v$  are

respectively a factor of  $\sim 8$  and  $\sim 3$  larger than the corresponding corrected ones).

When we now compare with determinations from other group catalogues, identified using similar FoF based algorithms, we can appreciate the extent of the effect (see Table 1 of Merchán & Zandivarez 2004). The typical median values, resulting from different group catalogues that do not take into account this effect, are:  $\bar{M}_v \simeq 5.5 \times 10^{13} h_{72}^{-1} M_\odot$  and  $\bar{R}_v \simeq 1.4 h_{72}^{-1} \text{Mpc}$ . In order to avoid such effects Tago et al. (2006) choose to use a constant in redshift FoF linking parameter. However, the decrease of the redshift selection function of the 2dF parent galaxy catalogue implies that they select intrinsically different type of groups as a function of redshift (ie., at higher redshifts they will tend to select more centrally condensed groups or the centers of clusters that have a high enough central density to survive the drop of the selection function at their distance).

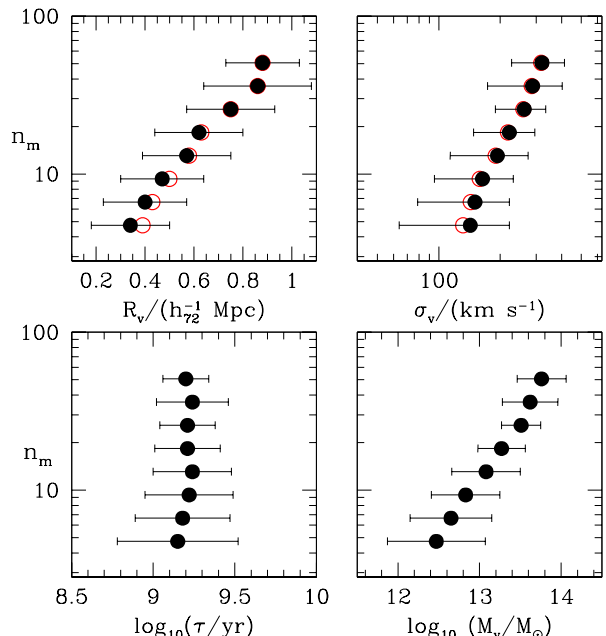


FIG. 7.— 2PIGG group virial radius (upper left panel), the velocity dispersion (upper right panel), the corresponding group crossing time (lower left) and the group virial mass (lower right) as a function of group “richness” ( $n_m$ ). The open circles correspond to the raw values and filled circles to the discreteness corrected values. Note, that here we allow also  $n_m > 30$  groups.

It is important to note that although the presented median values of the various dynamical group parameters are useful in order to compare with other studies, they are rather ill-defined, since we are mixing groups of different richness which could have distinct morphological and dynamical characteristics. Indeed, this is the case and in Fig.7 we present the correlation between various dynamical and morphological group parameters with group “richness” ( $n_m$ ). It is evident that there are very significant correlations of the group size, velocity dispersion and virial mass with  $n_m$ . A least square fit to the corrected, for the redshift-bias and discreteness effects, data ( $n_m \geq 4$ ) gives:

$$\begin{aligned} \sigma_v / \text{km s}^{-1} &\simeq 4.83(\pm 0.26)n_m + 122(\pm 3) \\ R_v / (h_{72}^{-1} \text{Mpc}) &\simeq 0.0212(\pm 0.0008)n_m + 0.254(\pm 0.007) \\ \log_{10}(M_v / M_\odot) &= 0.0416(\pm 0.0018)n_m + 12.36(\pm 0.02). \end{aligned}$$

The above trends of the group projected size, velocity dispersion and virial mass could be a natural consequence of the hierarchy of cosmic structures.

It is also evident from Fig. 7 that the 2PIGG groups have consistent crossing times, independent of the number of galaxy members, of  $\sim 1.5$  Gyr's which implies that the majority of them could be virialized systems (except probably for those formed within the last few Gyrs). Had we used instead of the virial radius the de-projected  $r_{\max}$  value we would have found a median crossing time of  $\sim 3.8$  Gyrs, still significantly smaller than the age of the universe.

## 5. CONCLUSIONS

Using Monte-Carlo and N-body simulations we have investigated the different biases that enter in the determination of the 2PIGG morphological and dynamical characteristics and we have devised statistical correction procedures to recover their bias free values.

Within a redshift that the 2PIGG groups have a roughly constant space number density ( $z \leq 0.08$ ), we derived the average morphological and dynamical characteristics (size, velocity dispersion, virial mass and crossing times), which

we find to be significantly smaller than those of other recent studies, exactly because we have taken into account the redshift-dependant bias. Within  $z \leq 0.08$ , the median value of the group virial radius, virial mass and crossing time is  $\sim 6 \times 10^{12} h_{72}^{-1} M_{\odot}$ ,  $\sim 0.4 h_{72}^{-1}$  Mpc and  $\sim 1.5$  Gyr's, respectively.

Assuming that groups constitute a homogeneous spheroidal population, we numerically invert the projected, discreteness free, axial ratio distribution to obtain the corresponding intrinsic one. The only acceptable model is that of a prolate, or a triaxial with pronounced prolatness, distribution with a mean axial ratio of  $\beta \simeq 0.46$  and a dispersion of  $\sim 0.16$ .

We have also found that there is a correlation of the size and the velocity dispersion with the number of group members, which is probably a natural outcome of the hierarchy of cosmic structures.

## ACKNOWLEDGEMENTS

C.Ragone-Figueroa acknowledges financial support by the LENAC network and thanks INAOE for its hospitality. We also thank the referee, T. Goto, for useful suggestions.

## REFERENCES

- Allgood, B., Flores, R.A., Primack, J.R., Kravtsov, A.V., Wechsler, R.H., Faltenbacher, A., Bullock, J.S., 2006, MNRAS, 367, 1781  
 Basilakos, S., Plionis, M., Maddox, S.J., 2000, MNRAS, 316, 779  
 Basilakos, S., Plionis, M., Rowan-Robinson, M., 2001, MNRAS, 323, 47  
 Bahcall, N., et al., 2003, ApJS, 148, 243  
 Berlind, A.A., et al., 2006, astro-ph/0601326  
 Carter, D. & Metcalfe, N., 1980, MNRAS, 191, 325  
 Cooray, R.A., 2000, MNRAS, 313, 783  
 de Lapparent, V., Geller, M.J., Huchra, J.P., 1991, ApJ, 369, 273  
 de Theije, P.A.M., Katgert, P. & van Kampen, E. 1995, MNRAS, 273, 30  
 Diaferio, A., Kauffmann, G., Colberg, J.M. & White, S.D.M., 1999, MNRAS, 307, 537  
 Eke, V.R., et al., 2004, MNRAS, 348, 866  
 Fall, M. & Frenk, C. S., 1983, ApJ, 88, 1626  
 Franx, M., Illingworth, G., de Zeeuw, T., ApJ, 383, 112 (1991)  
 Frederic, J.J., ApJS, 97, 259 (1995)  
 Gal, R.R., de Carvalho, R.R., Lopes, P.A.A., Djorgovski, S.G., Brunner, R.J., Mahabal, A., Odewahn, S.C., 2003, AJ, 125, 2064  
 Goto, T., et al., 2002, AJ, 123, 1807  
 Hubble, E.P., 1926, ApJ, 64, 321  
 Jaaniste, J., Tago, E., Einsato, M., Einsato, J., Andernach, H., Mueller, V., 1998, A&A, 336, 35  
 Jing, Y.P., Suto, Y., 2002, ApJ, 574, 538  
 Kasun, S.F. & Evrard, A.E., 2005, ApJ, 629, 781  
 Lee, B.C., et al., 2004, AJ, 127, 1811  
 Lopes, P.A.A., de Carvalho, R.R., Gal, R.R., Djorgovski, S.G., Odewahn, S.C., Mahabal, A.A., Brunner, R.J., 2004, AJ, 128, 1017  
 Merchán, M.E., Zandivarez, A., 2002, MNRAS, 335, 216  
 Merchán, M.E., Zandivarez, A., 2005, ApJ, 630, 759  
 Oleak H., Stoll D., Tiersch H., MacGillivray H.T. 1995, AJ, 109, 1485  
 Paz, D.J., Lambas, D.G., Padilla, N., Merchán, M., 2006, MNRAS, 366, 1503  
 Plionis M., Barrow J.D., Frenk, C.S., 1991, MNRAS, 249, 662  
 Plionis M., Valdarnini, R., Jing, Y.P., 1992, ApJ, 398, 12  
 Plionis, M., Basilakos, S. & Tovmassian, H., 2004, MNRAS, 352, 1323  
 Ramella, M., Geller, M.J., Pisani, A., & da Costa, L.N., 2002, AJ, 2976, 123  
 Ryden S.B., 1996, ApJ, 461, 146  
 Sandage, A., Freeman, K.C. & Stokes, N.R., ApJ, 160, 831 (1970)  
 Sathyaprakash, B.S., Sahni, V., Shandarin, S.; Fisher, K.B., 1998, ApJ, 507, L109  
 Sereno, M., De Filippis, E., Longo, G., Bautz, M.W., 2006, astro-ph/0602051  
 Springel, V., 2005, MNRAS, 364, 1105  
 Tremblay, B., & Merrit, D., 1995, AJ, 110, 1039  
 Tago, E., Einasto, J., Saar, E., Einasto, M., Suhhonenko, I., Joeveer, M., Vennik, J., Heinämäki, P., Tucker, D.L., 2006, AN, 327,365  
 Valdarnini, R., Ghizzardi, S., Bonometto, S., 1999, NewA, 4, 71  
 Vio, R., Fasano, G., Lazzarin, M., Lessi, O., 1994, A&A, 289, 640  
 Zeldovich, Ya. B., Einasto, J., Shandarin, S., 1982, Nature, 300, 407

TABLE 1

THE MEDIAN DYNAMICAL CHARACTERISTICS OF 2PIGG GROUPS WITH  $4 \leq n_m \leq 30$ , FOR VARIOUS CUTS IN REDSHIFT AND FOR THE REDSHIFT BIAS CORRECTED AND UNCORRECTED CASES. WE ALSO PRESENT THE UNCORRECTED CASE FOR THE VERY LOCAL VOLUME ( $z \leq 0.03$ ), WHERE THE REDSHIFT BIAS IS INEXISTENT.

$z$	#	Correct bias	$\bar{\sigma}_v/\text{kms}^{-1}$	$\bar{M}_v/h_{72}^{-1}M_{\odot}$	$\bar{R}_v/h_{72}^{-1}\text{Mpc}$	$\bar{r}_{\max}/h_{72}^{-1}\text{Mpc}$	$\bar{\tau}/\text{yr}$
$\leq 0.08$	1728	Yes	$150 \pm 34$	$5.7 \times 10^{12}$	0.38	0.73	$1.5 \times 10^9$
$\leq 0.03$	199	No	$157 \pm 35$	$6.2 \times 10^{12}$	0.40	0.75	$1.3 \times 10^9$
$\leq 0.08$	1728	No	$188 \pm 45$	$1.4 \times 10^{13}$	0.62	1.05	$1.9 \times 10^9$
$\leq 0.2$	6128	No	$257 \pm 70$	$4.2 \times 10^{13}$	0.98	1.71	$2.2 \times 10^9$